Theoretical studies of optimal light delivery for tumor treatment

Lihong V. Wang, Wei R. Chen, Robert E. Nordquist

Lihong V. Wang, Wei R. Chen, Robert E. Nordquist, "Theoretical studies of optimal light delivery for tumor treatment," Proc. SPIE 2975, Laser-Tissue Interaction VIII, (16 June 1997); doi: 10.1117/12.275462

SPIE.

Event: BiOS '97, Part of Photonics West, 1997, San Jose, CA, United States

Theoretical Studies of Optimal Light Delivery for Tumor Treatment

Lihong Wang, Ph. D.
Bioengineering Program, Texas A&M University
College Station, Texas 77843-3120
Tel: (409) 847-9040; Fax: (409) 847-9005
E-mail: LWang@tamu.edu; URL: http://biomed.tamu.edu/~lw

Wei R. Chen, Ph. D.
Oklahoma School of Science and Mathematics
1141 North Lincoln Boulevard, Oklahoma City, OK 73104
and
Department of Physics and Astronomy, University of Oklahoma
Norman, OK 73109

Robert E. Nordquist, Ph. D.
Wound Healing of Oklahoma, Inc.
3939 N. Walnut Street
Oklahoma City, OK 73105

ABSTRACT

Optimal laser light delivery into turbid biological tissues was studied using Monte Carlo simulations. The goal was to efficiently deliver maximum amount of optical power into buried tumors being treated while avoiding damage to normal tissue caused by strong optical power deposition underneath the tissue surface illuminated by the laser beam. The buried tumors were considered to have much higher absorption than the surrounding normal tissue via selective uptake of absorption-enhancement dye by the tumor. The power delivering efficiency to buried tumors was investigated for various diameters of the laser beam. An optimal beam diameter was estimated to achieve the maximum product of the power coupling efficiency and the power delivered to the buried tumor. The distribution of power deposition was simulated for single beam delivery and multiple beam delivery as well. The simulated results showed that with an appropriate dye enhancement and an optimal laser delivery configuration, a high selectivity for laser treatment of tumor could be achieved.

KEY WORDS

Monte Carlo, light delivery, optical therapy, turbid media, biological tissues.

SPIE Vol. 2975 • 0277-786X/97/$10.00

INTRODUCTION

Laser-tissue interactions and their therapeutic applications is a fast growing research area. Biological tissues are turbid media, in which light attenuates rapidly because of light absorption augmented by strong light scattering. As a consequence, deeply buried tumors usually receive much less optical power than the subsurface normal tissues, which hampers efficacious optical treatment of tumors. By maximizing the power delivered to the target tumors while avoiding damaging subsurface normal tissues, laser treatments may be improved in several aspects. First, the absorption coefficient of tumors may be significantly increased by infusing dyes into the tumors. Secondly, the wavelength of the laser light may be selected to maximize the ratio between the absorption of the tumor and that of the surrounding normal tissue. Thirdly, the light delivery scheme may be optimized to maximize the power absorption by the target tumors. We will concentrate on the third approach in this paper.

Previous studies have investigated the effect of the diameter of the laser beam while the power density of the laser beam was kept constant.[1,2] In this paper, Monte Carlo simulations were used to identify the optimal diameters of the laser beam and to investigate the effect of multiple beam delivery compared with single beam delivery under the condition that the location of the buried tumor is known and the absorption of the tumor is enhanced.

METHOD

Monte Carlo simulations of light transport in tissues have been implemented previously for simple tissue geometry.[3-7] To compute light distributions according to the tissue geometry and optical properties, including refractive index n, absorption coefficient μ_a, scattering coefficient μ_s, and anisotropy factor g, we have written a Monte Carlo program in C for tissues with buried objects. We used the delta-scattering technique[8] for photon tracing to greatly simplify the algorithm because this technique allows a photon packet to be traced without directly dealing with photon crossings of interfaces between different types of tissues. This technique can be used only for refractive-index-matched tissues, although it allows the ambient clear media (e.g., air) and the tissue to have mismatched refractive indices.

We assume that the tissue system has multiple tissue types with identical refractive indices. The interaction coefficient of the *i*th tissue type, defined as the sum of μ_a and μ_s, is denoted by μ_i. The technique is briefly summarized as follows.

1. Define a majorant interaction coefficient μ_m, where $\mu_m \geq \mu_i$ for all i.
2. Select a step size R between two consecutive interactions based on the majorant interaction coefficient,

$$R = - \ln(\xi) / \mu_m, \tag{1}$$

where ξ is a uniformly distributed random number between 0 and 1 ($0 < \xi \leq 1$). Then, determine the tentative next collision site $\mathbf{r}_k'$ by:

$$\mathbf{r}_k' = \mathbf{r}_{k-1} + R\, \mathbf{u}_{k-1}, \tag{2}$$

where $\mathbf{r}_{k-1}$ is the current site and $\mathbf{u}_{k-1}$ is the direction of the flight.

3. Play a rejection game:

a. Get a random number η, which is a uniformly distributed random number between 0 and 1 ($0 < \eta \leq 1$).
a. If $\eta \leq \mu_i(\mathbf{r}_k')/\mu_m$, i.e., with a probability of $\mu_i(\mathbf{r}_k')/\mu_m$, accept this point as a real interaction site ($\mathbf{r}_k = \mathbf{r}_k'$).
b. Otherwise, do not accept $\mathbf{r}_k'$ as a real interaction site but select a new path starting from $\mathbf{r}_k'$ with the unchanged direction $\mathbf{u}_{k-1}$ (i.e., set $\mathbf{r}_{k-1} = \mathbf{r}_k'$ and return to Step 2).

The treatment of photon tracing after step 3 is similar to that in Ref. 7 and will not be repeated here.

The validity can be easily understood by introducing an imaginary interaction event that changes neither the weight nor the direction of the photon. This definition implies that such imaginary interactions are not physically observable, i.e., they can be introduced with any interaction coefficient at any point. We may assume that the majorant interaction coefficient μ_m is a sum of the real μ_{re} and imaginary μ_{im} interaction coefficients, where the real interaction coefficient is μ_{re} is $\mu_i(\mathbf{r}_k')$. In the procedure outlined above, a fraction of the interactions,

$$1 - \mu_{re}/\mu_m = \mu_{im}/\mu_m \tag{3}$$

are imaginary interactions. From another point of view, it is easy to see that on the average, for every μ_m total interactions, there will be μ_{re} interactions accepted as real interactions. The mean free path for the majorant interactions in the delta-scattering method is $1/\mu_m$, and the mean free path for the real interactions in the direct method is $1/\mu_{re}$. Therefore, the photon will move to the correct interaction site using the delta-scattering technique as it would using the direct method because

$$\mu_m(1/\mu_m) = \mu_{re}\,(1/\mu_{re}), \tag{4}$$

where the left-hand side means the average distance traveled by the photon packet with μ_m total steps or with μ_{re} real interactions in the delta-scattering method, and the right-hand side means the average distance traveled with μ_{re} real interactions in the direct method.

During the tracing of each weighted photon,[7] the light absorption, reflection, or transmission were correspondingly scored into different arrays according to the spatial positions of the photon. Multiple photons are traced to achieve an acceptable statistical variation. For this study, 100,000 photons were traced.

This Monte Carlo program was used to simulate power deposition for tissue configurations as shown in Fig. 1. Fig. 1(a) shows a single beam delivery scheme to a tissue slab with a tumor buried in the center. The lateral dimensions in the xy-plane was considered optically infinite, i.e., much greater than the penetration depth of light. Fig. 1(b) illustrates a multiple beam delivery scheme to a tissue cube with a tumor buried in the center. One or more of the four beams may be selected to illuminate the tissue while the other beams were blocked.

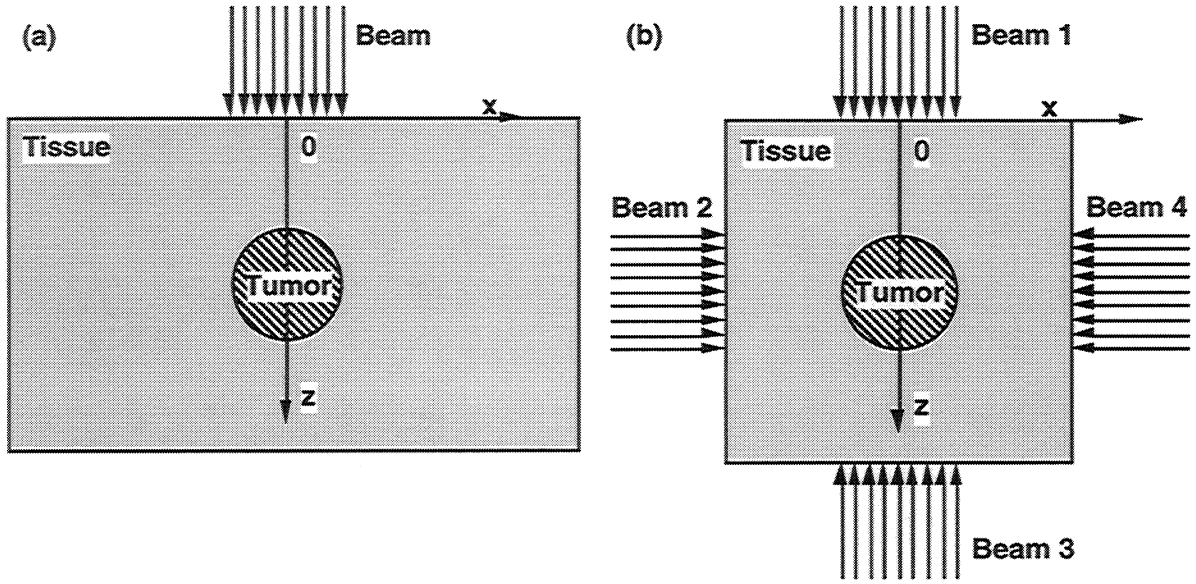

Fig. 1. Configurations of the biological tissue and laser beams: (a) single beam delivery to a wide tissue slab and (b) multiple beam delivery to a tissue cube. The tumor was a sphere that was centered in the background tissue and aligned with the center of the laser beam. In both cases, the optical properties of the background tissue were: absorption coefficient μ_a = 0.1 cm^{-1}, scattering coefficient μ_s = 100 cm^{-1}, anisotropy g = 0.9. The optical properties of the tumor were: μ_a = 1 cm^{-1}, μ_s = 100 cm^{-1}, g = 0.9. The diameter of the tumor was 1 cm. The thickness of the tissue slab in (a) and the side of the tissue cube in (b) were both 3 cm.

RESULTS

The single beam delivery scheme as shown in Fig. 1(a) was studied using the Monte Carlo program. The total power absorption by the buried tumor P_{tumor} in W and the maximum deposited power density in the tissue Q_{max} in W/cm^3 were simulated for different radii of the laser beam while the total incident power P_s was kept constant (Fig. 2).

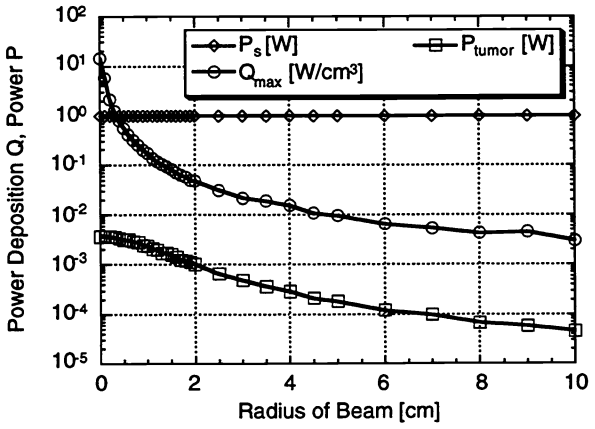

Fig. 2. Power absorption P_{tumor} by the tumor and maximum power deposition Q_{max} as a function of the radius of the laser beam in single beam delivery to a tissue slab while the total power of the incident laser beam P_s was set to 1 W.

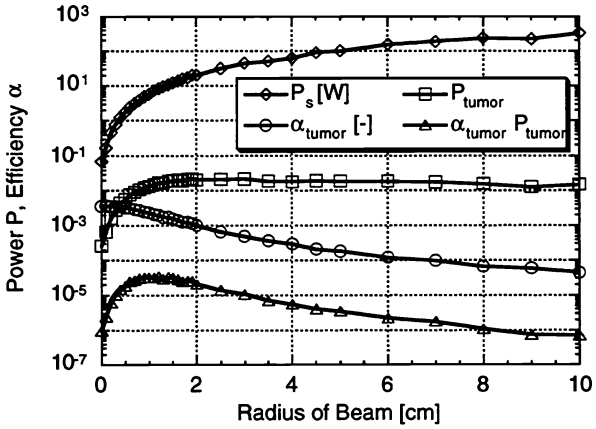

Fig. 3. (1) Power of the incident laser beam P_s (diamonds), (2) power absorption by the tumor P_{tumor} (squares), (3) power coupling efficiency α_{max} (circles), and (4) product of the power coupling efficiency and power absorption by the tumor $\alpha_{tumor} P_{tumor}$ (triangles), as a function of the radius of the laser beam in single beam delivery to a tissue slab while the maximum power deposition Q_{max} was kept at 1 W/cm^3.

In determining the maximum power density deposited in the tissue immediately under the laser beam, P_s was set to 1 W for convenience. After the data point at zero radius of beam was removed, the following relationship was fitted using least-squares fit.

$$Q_{max} = 0.156\ r^{-1.70} \tag{5}$$

where r was the radius of the beam in cm, and Q_{max} was in W/cm^3. Since the incident power P_s was set to 1 W in this simulation, P_{tumor} was equal to the fraction of the incident power that was absorbed by the tumor, α_{tumor}, where α_{tumor} was defined as the ratio between P_{tumor} and P_s, i.e., the efficiency of power coupling from the incident laser beam into the tumor.

The power absorption by the buried tumor P_{tumor} was also simulated for different radii of the laser beam while the total incident power P_s was varied to keep the maximum power deposition Q_{max} constant (Fig. 3). For convenience, Q_{max} was set to 1 W/cm^3. The product of α_{tumor} and P_{tumor} was also shown in Fig. 3. There existed an optimal radius of the laser beam to maximize this product, where the optimal radius was between 1 and 1.5 cm for this tissue configuration.

An analytical estimate of the optimal radius may be obtained using the geometry in Fig. 4. The dashed horizontal line underneath the tissue surface was one transport mean free path L_t' below the surface. To the first-order approximation, the laser beam may be modeled as isotropic point sources one transport mean free path below the surface.[9,10] The coupling efficiency of power from these equivalent point sources to the tumor varied with the horizontal positions of the point sources. The coupling efficiency was the greatest at the center (x = 0) and decreased as x increased. When the distance between the point source and the center of the tumor was increased by one penetration depth δ compared with the shortest distance at x = 0, the contribution of the point source would be significantly reduced. The horizontal coordinate corresponding to this distance was used to estimate the optimal radius of the laser beam r_o. The optimal radius was derived as

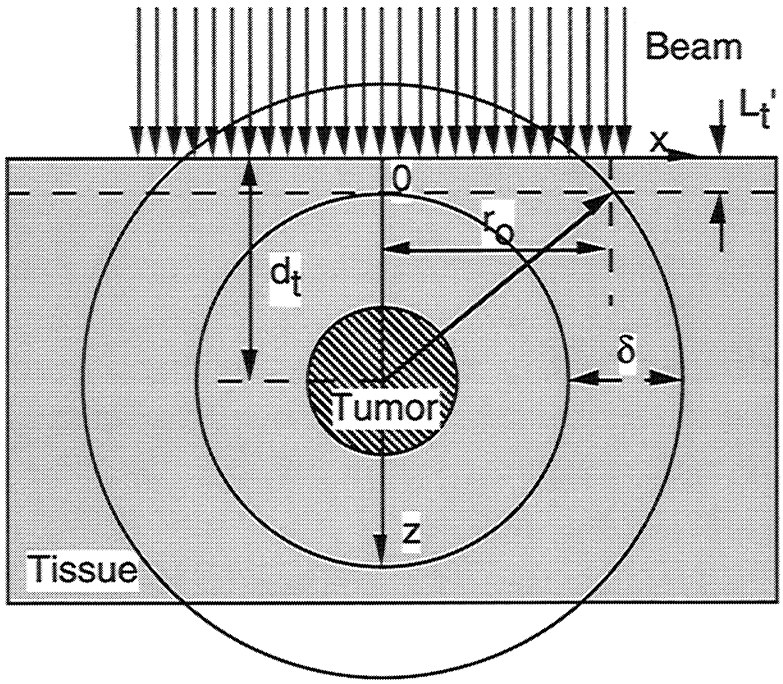

Fig. 4. Schematic of single beam delivery for the derivation of the estimated optimal radius of the laser beam.

$$r_o = \sqrt{\delta\ (2d_t - 2L_t' + \delta)} \tag{6}$$

where d_t was the distance between the center of the tumor and the upper tissue surface, and δ was the penetration depth.

The multiple beam delivery scheme as shown in Fig. 1(b) was studied using this Monte Carlo program. The distributions of power deposition are shown in Figs. 5-7 for beam radii of 0, 0.5 cm, and 1 cm, respectively. The power of each beam was set to 1 W for convenience. The plots in Figs. 5-7 described the $\log_{10}$(absorption), where the absorption was the power deposition in the units of W/cm^3. The general trend was that the more beams turned on for the light delivery, the more homogeneous and intense the power deposition in the tumor was. The broader the beams, the more homogeneous the power deposition in the tumor while it would be most effective if the optimal radius as described by Eq. 6 was chosen.

CONCLUSIONS and DISCUSSION

Fig. 2 showed that the maximum power deposition Q_{max} decreased with increased beam size as the total power of the incident laser beam was kept constant. As the beam broadened, the edge of the beam contributed less and less to the maximum power deposition Q_{max}. The relationship between the maximum power deposition and the radius of the beam was described by the empirical express in Eq. 5. The power density ϕ of the laser beam was inversely proportional to the area of the beam while the total power of the beam was kept constant. Eq. 5 may be reformulated as follows.

$$Q_{max} = 0.156\ r^{-1.70} = 0.156\ (r^{-2})^{0.85} \propto \phi^{0.85} \quad (7)$$

Therefore, the maximum power deposition Q_{max} was not proportional to the power density ϕ as one might have imagined.

Although Fig. 2 was generated for P_s = 1 W, the figure may be scaled according to the actual power P_s. If the actual power P_s of the laser was fixed, an appropriate radius of beam had to be selected to ensure the maximum power deposition Q_{max} was below the damage threshold Q_{th}.

Fig. 3 showed that when the maximum power deposition Q_{max} was kept constant below the damage threshold Q_{th}, the total power of the incident laser beam increased with the radius of the beam. The power deposited into the tumor P_{tumor} increased rapidly with the increased beam size but gradually reached a plateau for radius greater than 1 cm. The efficiency of power transfer α_{tumor} from the incident laser beam to the tumor decreased with the radius of the beam. The product of α_{max} and P_{tumor} reached maximum near 1-1.5 cm radius.

The optimal laser beam radius, given in Eq. 6 and verified by our Monte Carlo simulation (see Fig. 3), is very useful for the laser therapy for deep tumors. By limiting the size of the beam, unnecessary exposure and heating of skin surface can be minimized. By expanding the beam, the damage caused by the peak power deposition ("hot spot") near the tissue surface can be avoided. By optimizing the beam size, the power of the incident laser beam is efficiently coupled into the tumor, and the power absorption by the tumor is nearly maximum.

The optimal radius may be estimated using Eq. 6 for the presented Monte Carlo simulations. The optical properties of the background tissue were: $\mu_a = 0.1\ cm^{-1}$, $\mu_s = 100\ cm^{-1}$, $g = 0.9$. The distance between the center of the tumor and the upper tissue surface d_t was 1.5 cm. Therefore, the transport mean free path was

$$L_t' = 1/[\mu_a + \mu_s\ (1 - g)] = 0.099\ cm \quad (8)$$

and the penetration depth was

$$\delta = \sqrt{3\ \mu_a[\mu_a + \mu_s(1 - g)]} = 0.57\ \ cm \quad (9)$$

The estimated optimal radius r_o was 1.39 cm, which was in good agreement with the product curve in Fig. 3.

Figs. 5-7 demonstrated the effect of multiple beam delivery. When a narrow beam was used, the power deposition under the beam was much stronger than that in the tumor. Therefore, it would be easy to cause damage to the tissue directly under the beam. When the radius of the beam broadened to 0.5 cm and 1 cm, the power deposition under the beam was reduced significantly.

In Fig. 7, the power deposition in the tumor was comparable with that under the beam. In all cases, multiple beam delivery, especially four beam delivery, had clear advantages over single beam delivery. Multiple beam delivery yielded a more homogeneous power deposition in the tumor and a higher power delivered to the tumor without causing damage to the surrounding normal tissue than single beam delivery.

In the simulations presented in this paper, the absorption coefficient of the buried tumor was assumed to be enhanced with dyes and reached ten times that of the background normal tissue. With the use of near-infrared lasers and matched dyes, this contrast may be further increased as in the case of 805 nm laser and indocyanine green[11-13] for photothermal interactions. The fact that the maximum power absorption by background tissue can be reduced with four beams to the level

comparable to that absorbed by the tumor shows the promise for better therapeutic outcomes by optimizing the configuration of light delivery. The further optimization can be achieved by increasing the concentration of the dyes in tumors. Surface cooling with liquid or gas can drastically reduce the energy accumulation on the surface tissue. Scanning the laser beams during the treatment can also be employed to reduce surface heating. It is also apparent that further increasing the number of beams would be beneficial.

Furthermore, when the total tumor direct killing is not the overriding objective, such as in the case of photothermal immunotherapy[14], the source power can be reduced to an even more tolerable level.

The rapid attenuation of light in turbid media can significantly reduce the energy reaching the target tumors. However, the optimal beam size, the enhanced tumor absorption, and a multiple beam delivery system can still allow the desired selectivity for target tissue as demonstrated by this study.

Although power has been used for this study, one can change the power to energy by replacing W with J and the conclusions apply to pulse laser beams as well. It is worth noting that this study only investigates the initial optical part of laser-tissue interactions. Once the optical power deposition in tissues is simulated, the power deposition may be used as the source term for further investigation into photothermal, photomechanical, or photochemical effects of interest.

SUMMARY

Monte Carlo simulations were proved to be a flexible and powerful tool in studying light transport in heterogeneous biological tissues. The studies of power deposition in buried tumors concluded that there existed an optimal radius of the laser beam to achieve both high power delivery efficiency and high power absorption by the tumor. An estimate of the optimal radius was given analytically. Multiple beam delivery was able to yield more homogeneous and greater power absorption by the tumor without causing damage to the normal tissues than single beam delivery. These results provide guidelines for various laser therapeutics including photothermal therapies, photomechanical therapies, and noninvasive photosensitizer-assisted laser therapies of deep tumors.

ACKNOWLEDGMENT

This project was sponsored in part by the National Institutes of Health grant R29 CA68562 and The Whitaker Foundation.

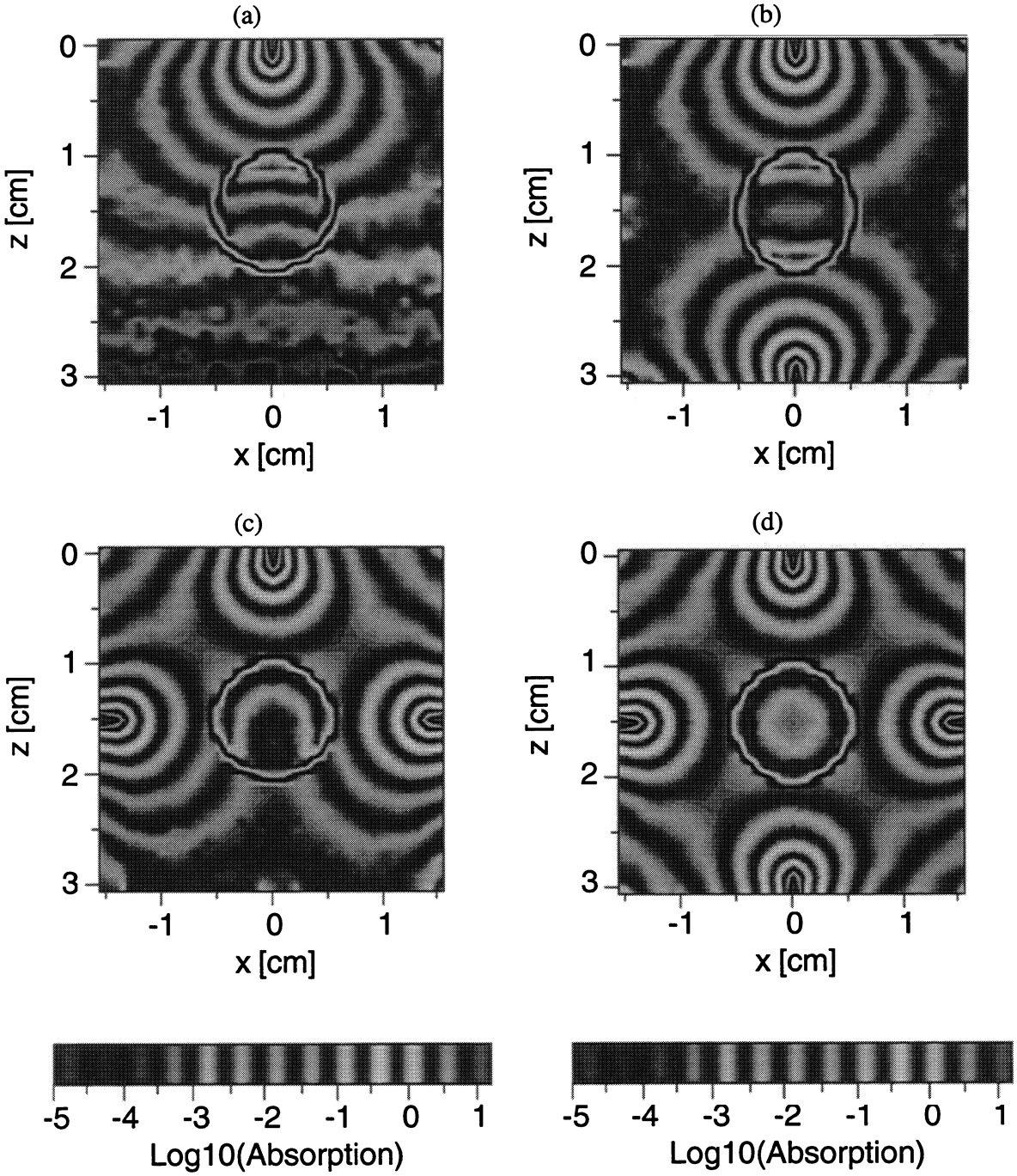

Fig. 5. False-color plots of the deposited power density distribution in W/cm^3 in the tissue cube in log scale for (a) 1 beam delivery, (b) 2 beam delivery, (3) 3 beam delivery, and (4) 4 beam delivery, where the radius of the beam was 0. The total power of the incident laser beam P_s was set to 1 W.

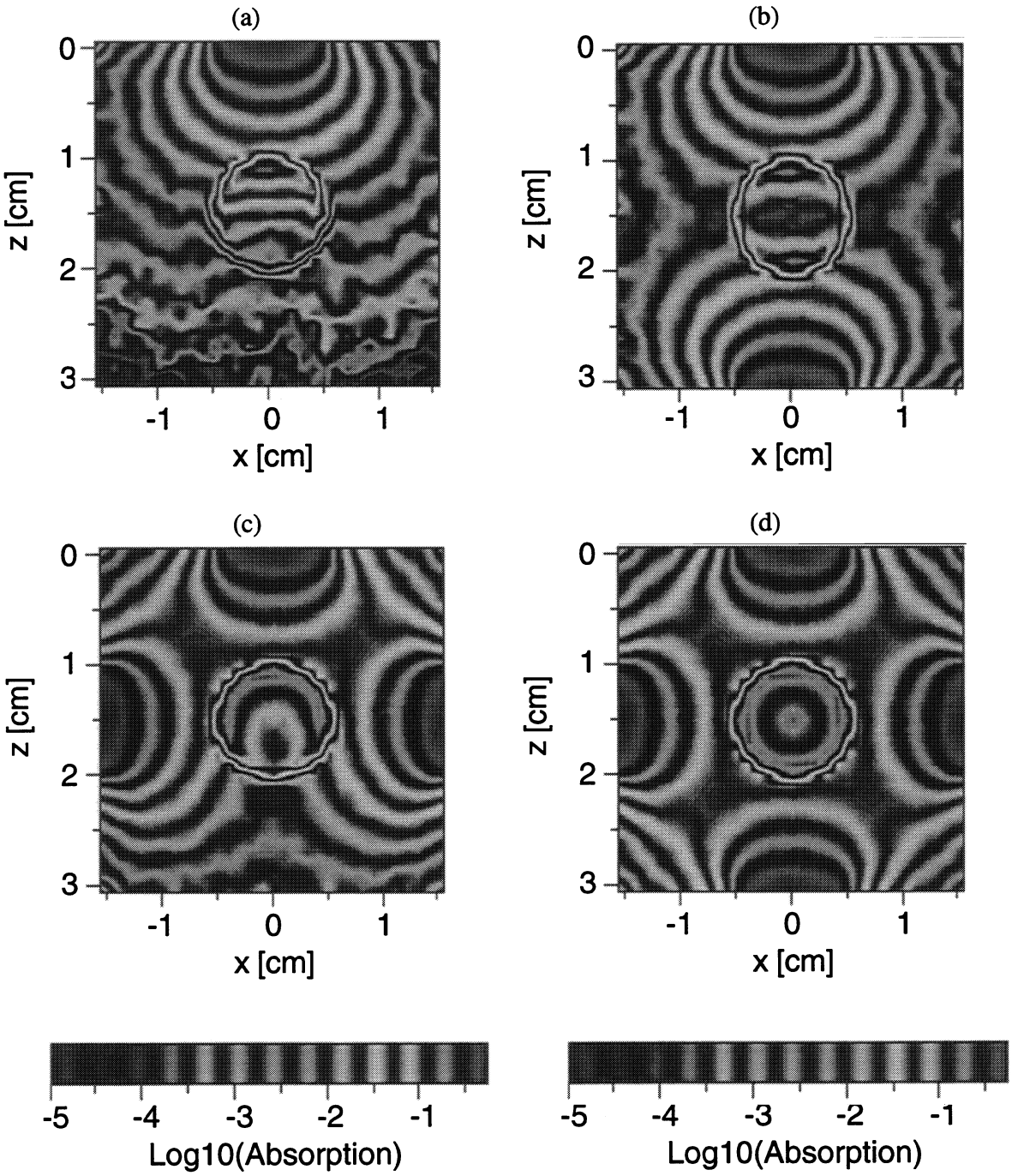

Fig. 6. False-color plots of the deposited power density distribution in W/cm^3 in the tissue cube in log scale for (a) 1 beam delivery, (b) 2 beam delivery, (3) 3 beam delivery, and (4) 4 beam delivery, where the radius of the beam was 0.5 cm. The total power of the incident laser beam P_s was set to 1 W.

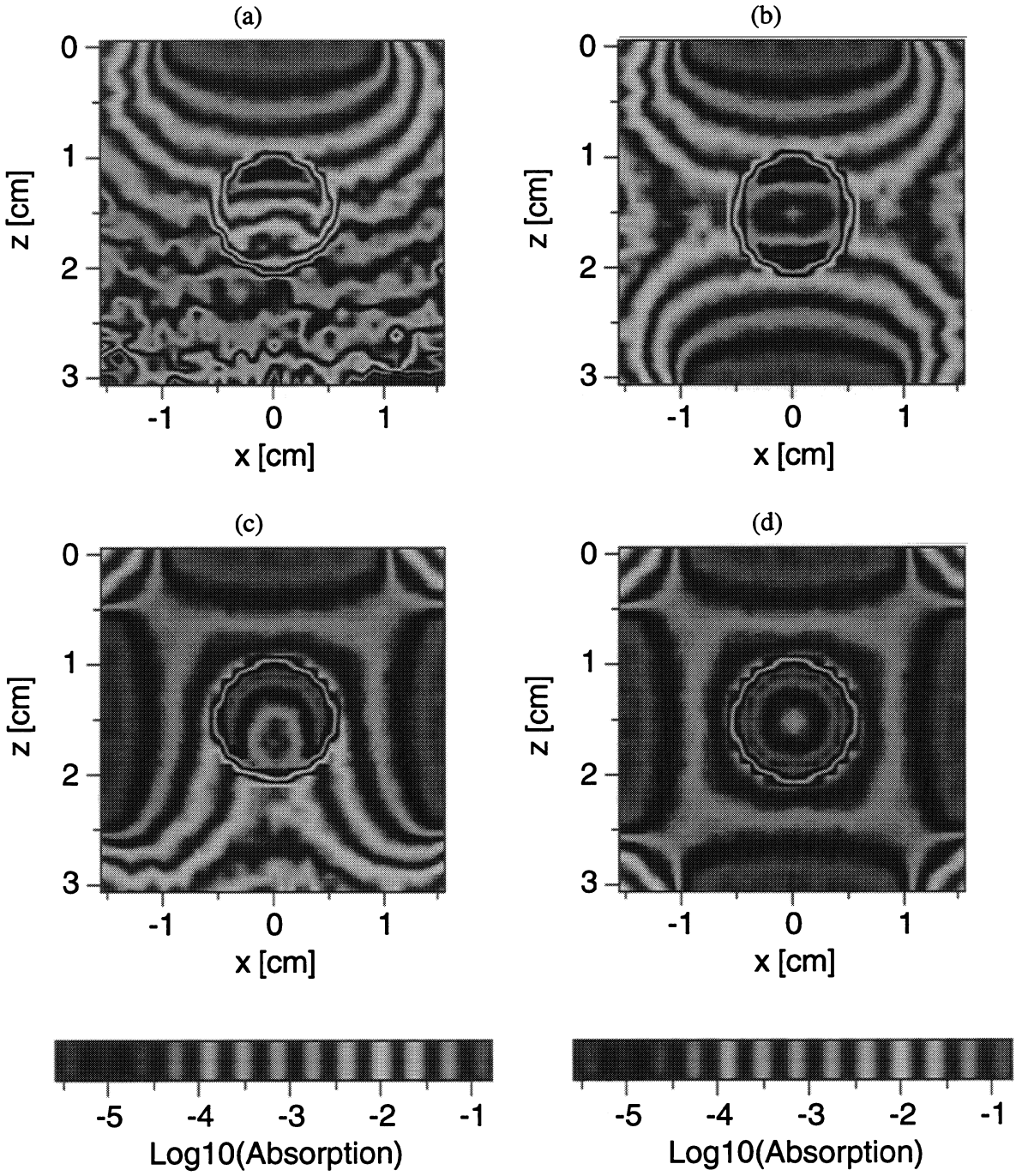

Fig. 7. False-color plots of the deposited power density distribution in W/cm^3 in the tissue cube in log scale for (a) 1 beam delivery, (b) 2 beam delivery, (3) 3 beam delivery, and (4) 4 beam delivery, where the radius of the beam was 1 cm. The total power of the incident laser beam P_s was set to 1 W.

REFERENCES

1. M. Keijzer, J. W. Pickering, and M. J. C. van Gemert, "Laser beam diameter for port wine stain treatment," Lasers in Surg. Med. **11**, 601-605 (1991).
2. Q. Chen, B. C. Wilson, M. O. Dereski, M. S. Patterson, M. Chopp, and F. W. Hetzel, "Effects of light beam size on fluence distribution and depth of necrosis in superficially applied photodynamic therapy of normal rat brain," Photochemistry & Photobiology **56**, 379-384 (1992).
3. B C Wilson and G A Adam, "Monte Carlo model for the absorption and flux distributions of light in tissue," Med. Phys. **10**, 824-830 (1983).
4. S. T. Flock, B. C. Wilson, D. R. Wyman, and M. S. Patterson, "Monte-Carlo modeling of light-propagation in highly scattering tissues I: model predictions and comparison with diffusion-theory," IEEE Trans. Biomed. Eng. **36**, 1162-1168 (1989).
5. S. A. Prahl, M. Keijzer, S. L. Jacques, and A. J. Welch, "A Monte Carlo model of light propagation in tissue," Proc. Soc. Photo-Opt. Instrum. Eng. **IS 5**, 102-111 (1989).
6. S. L. Jacques and L.-H. Wang, "Monte Carlo modeling of light transport in tissues," in Optical Thermal Response of Laser Irradiated Tissue, edited by A. J. Welch and M. J. C. van Gemert (Plenum Press, New York, 1995), pp. 73-100.
7. L.-H. Wang, S. L. Jacques, and L.-Q. Zheng, "MCML - Monte Carlo modeling of photon transport in multi-layered tissues," Computer Methods and Programs in Biomedicine **47**, 131-146 (1995). Note: The simulation software package can be downloaded from http://biomed.tamu.edu/~lw.
8. Lux and L. Koblinger, Monte Carlo Particle Transport Methods: Neutron and Photon Calculations (CRC Press, 1991).
9. T. J. Farrell, M. S. Patterson, and B. C. Wilson, "A diffusion theory model of spatially resolved, steady-state diffuse reflectance for the non-invasive determination of tissue optical properties in vivo," Med. Phys. **19**, 879-888 (1992).
10. L.-H. Wang and S. L. Jacques, "Use of a laser beam with an oblique angle of incidence to measure the reduced scattering coefficient of a turbid medium," Applied Optics **34**, 2362-2366 (1995).
11. W. R. Chen, R. L. Adams, S. Heaton, D. T. Dickey, K. E. Bartels, and R. E. Nordquist, "Chromophore-enhanced laser-tumor tissue photothermal interaction using an 808-nm diode laser," Cancer Letters **88**, 15-19 (1995)
12. W. R. Chen, R. L. Adams, K. E. Bartels, and R. E. Nordquist, "Chromophore-enhanced in vivo tumor cell destruction using an 808-nm diode laser," Cancer Letters, **94**, 125-131 (1995).
13. W. R. Chen, R. L. Adams, A. K. Higgins, K. E. Bartels, and R. E. Nordquist, "Photothermal effects on murine mammary tumors using indocyanine green and an 808-nm diode laser: an in vivo efficacy study," Cancer Letters, **98**, 169-173 (1995).
14. W. R. Chen, R. L. Adams, R. Carubelli, and R. E. Nordquist, "Laser-photosensitizer assisted immunotherapy: A novel modality for cancer treatment," Cancer Letter, in press (1997).